AIAA JOURNAL
Vol. 38, No. 4, April 2000

Analytical Predictions and Measurements of the Noise Radiated from Supersonic Coaxial Jets

Milo D. Dahl*
NASA John H. Glenn Research Center at Lewis Field, Cleveland, Ohio 44135-3191
and
Dimitri Papamoschou†
University of California, Irvine, Irvine, California 92717

The noise radiated from perfectly expanded coaxial jets was measured in an anechoic chamber for operating conditions with the same total mass flow and thrust and with the same temperature ratio. The shape of the measured noise spectrum at different angles to the jet axis was found to agree with spectral shapes for single, axisymmetric jets. Based on these spectra, the sound was characterized as being generated by large-scale turbulent structures or fine-scale turbulence. Modeling the large-scale structures as instability waves, a stability analysis was conducted for the coaxial jets to identify the growing and decaying instability waves in each shear layer and to predict their noise radiation pattern outside the jet. When compared to measured directivity, the analysis identified the region downstream of the outer potential core, where the two shear layers were merging, as the source of the peak radiated noise where instability waves, with their origin in the inner shear layer, reach their maximum amplitude. The changes in the measured noise directivity that occurred when the operating conditions were changed, holding mass flow and thrust constant, followed the trend predicted by the instability wave analysis.

I. Introduction

SUPERSONIC jet noise is generated by mechanisms associated with fine-scale turbulence, large-scale turbulent structures, and shocks. Depending on the jet operating conditions and the structure of the exhausting flowfield, each of these noise generating mechanisms can contribute to the noise radiated to the far field at a given frequency and in differing amounts as a function of the direction from the jet to the observer. Because jet noise continues to be of concern in the development of advanced aircraft, it is hoped that a greater understanding of the jet noise generation process will lead to means by which the noise may be reduced while maintaining acceptable propulsion system performance.

One concept for reducing supersonic jet noise is to replace the single-stream jet with a dual-stream, coaxial jet. Recent separate studies have considered this concept analytically[1] and experimentally.[2] The initial conditions used in these studies set the jet for shock-free, perfectly expanded flow. The resulting noise is generated by turbulent mechanisms that primarily radiate noise toward the downstream arc of the jet. If the jet speed is sufficiently supersonic, the large-scale turbulent structures become dominant noise radiators when their phase velocity is supersonic relative to the speed of sound in the adjacent lower-speed or ambient flow. The addition of a lower-speed secondary flow to a single supersonic jet modifies the growth rate and phase velocity of the large structures in the primary flow shear layer and, if the jet conditions are properly chosen, it has been shown experimentally that applying the secondary flow can lead to lower levels of radiated noise.[3]

For noise generated by large-scale structures, the analysis uses the instability wave noise generation model. The large-scale structures that exist in the growing jet shear layer are modeled as instability waves that initially grow rapidly and then decay in the axial direction as the shear layer widens. Tam and Burton[4] developed a matched asymptotic solution for the noise radiated from the instability waves in the slowly growing shear layer of a single-stream, supersonic, axisymmetric jet. The equations developed were used to calculate the stability characteristics and the radiated noise directivity of an instability wave at a single frequency and a single mode number. Their results showed good comparisons with measurements from low-Reynolds-number jet experiments. Comparisons of calculated results with measured data were also made with high-speed jets[5] and high-temperature jets.[6] This single-mode method was later extended to include the addition of multiple modes using stochastic theory.[7]

The instability wave noise generation model was applied to supersonic coaxial jets by Dahl and Morris.[1] The ability to complete the stability and noise calculations depended on computing numerically the mean flow for both velocity and density fields.[8] Thus, a variety of jet operating conditions could be modeled, including both normal and inverted velocity profiles, and the stability and noise generation could be studied due to velocity and density ratio changes between the two jet streams and area ratio changes at the nozzle exit. The results were focused on the Kelvin–Helmholtz-type inflectional instabilities. Other modes can exist in supersonic jets that may or may not radiate noise.[9] Using the eigenvalue problem approach of the instability wave model, each of these modes would have to be found and investigated separately to determine any ability for them to radiate noise. Direct numerical calculations, such as those proposed by Hixon et al.,[10] allow all radiating modes to develop naturally. The present paper is restricted to single-mode calculations.

Recently, Papamoschou[2] began small-scale experiments using perfectly expanded coaxial jets. The purpose was to explore flow conditions where Mach wave radiation is reduced from that of a single jet when a secondary stream is applied at proper conditions. Mach wave radiation comes from the dominant noise generated by instability waves convecting supersonically in the shear layer of a jet. It can be generated by both the Kelvin–Helmholtz-type and the supersonic-type instability modes. According to the model presented by Papamoschou, if the relative phase velocities of the Mach wave generating disturbances can be made subsonic in both shear layers, then Mach wave radiation can be reduced. The success of this approach has been shown in flow visualizations[2] and in acoustic field measurements.[3]

The experimental facilities that have been built allow acoustic data to be taken for noise generated by perfectly expanded coaxial jets, a condition on which the instability wave theory for coaxial jets is based. At the time the initial analytical study of coaxial jets was completed, no sets of noise measurements of perfectly expanded,

Received 5 February 1999; revision received 27 July 1999; accepted for publication 4 August 1999.

*Research Scientist, Structures and Acoustics Division. Member AIAA.
†Professor, Department of Mechanical and Aerospace Engineering. Member AIAA.

coaxial jets were known to exist to compare with predictions. Thus, the opportunity exists to compare the calculated analytical results to measured data where Mach wave radiation exists. In the next section, the experimental method is described for setting up and measuring the noise from perfectly expanded, supersonic, coaxial jets. This is followed by a description of the characteristics of the measured noise spectra and noise levels in the far field of the jet. The behavior of the noise levels with changing operating conditions is shown to be consistent with what is expected for normal-velocity-profile jets at constant mass flow, thrust, and exit area conditions. The spectra suggest that large-scale turbulent structures are the dominant source of noise radiated in the downstream direction. This latter characteristic is used to justify using the instability wave noise generation model to determine the source of this radiated noise. After a brief description of the instability wave model, results from a stability analysis are used to describe the dominant source region. Finally, comparisons are made between predicted and measured noise radiation directivity patterns.

II. Experimental Method

Experiments were conducted in a coaxial jet facility with the capability of supplying mixtures of helium and air to the inner and outer flows (Fig. 1). The inner nozzles, of 12.7-mm exit diameter, were designed by the method of characteristics for Mach numbers 1.5, 1.75, and 2.0. The outer nozzle formed a smooth contraction terminating in an exit diameter of 21.6 mm. Both flows exhausted into ambient, still air. Details of the facility can be found in Ref. 2.

Helium–air mixtures allow variation of the gas constant R and, thus, of the velocity at fixed Mach number and fixed total temperature. A jet composed of a helium–oxygen mixture simulates very accurately the speed of sound, velocity, and growth rate of a hot jet at the same density ratio.[2] In this experiment, the mixtures were accurately metered so that the uncertainty in the gas constant was less than 5%. For all cases, the total temperature of the gas mixture was around 300 K. The exit density can be translated to the temperature of the simulated hot jet via the relation $T/T_\infty = \rho_\infty/\rho$. The experimental Mach numbers, velocity ratios, and simulated temperature ratios are shown in Table 1. Typical Reynolds numbers in the experiments were 5×10^5 for the inner flow, based on jet diameter, and 5×10^4 for the outer flow, based on annulus thickness.

The jet noise was recorded by a $\frac{1}{8}$-in. condenser microphone connected to a preamplifier and power supply (Bruel and Kjaer Models 4138, 2670, and 5935L, respectively). The microphone has a frequency response up to 150 kHz and was sampled at 400 kHz by a fast analog-to-digital board (National Instruments AT-MIO-16E1) installed in a Pentium Pro computer. Each recording consisted of 54,280 samples (135 ms), corresponding to passage of about 10,000 eddies the size of the inner-jet diameter. The signal was high-pass filtered at 500 Hz by a Butterworth filter to remove spurious low-frequency noise. The power spectrum of each recording was computed using a 1024-point fast Fourier transform with a full Hanning window. The microphone was calibrated daily before each series of recordings (Bruel and Kjaer Model 4231 calibrator).

Table 1 Operating conditions for supersonic coaxial jet calculations

Case	M_1	T_1/T_∞	M_2	T_2/T_∞	U_2/U_1
CM1[a]	1.50	3.03	1.09	1.89	0.58
CM2[a]	1.75	2.64	0.88	1.65	0.40
CM3[a]	2.00	1.89	0.52	1.18	0.22
CT1[b]	2.00	3.33	0.50	2.76	0.23
CT2[b]	2.00	3.33	0.80	2.76	0.37
CT3[b]	2.00	3.33	0.95	2.76	0.44

[a]Constant mass flow and thrust.
[b]Constant temperature ratio.

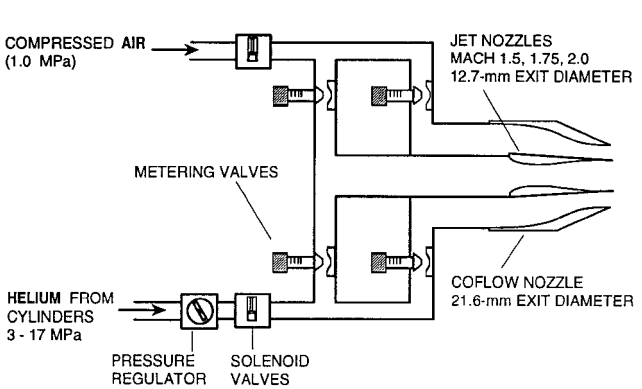

Fig. 1 Schematic of the supersonic coaxial jet facility.

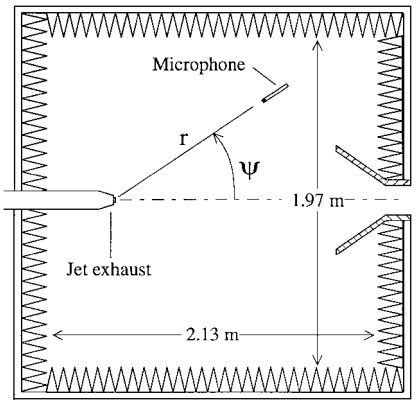

Fig. 2 Anechoic chamber and positioning of jet and microphone.

Sound measurements were conducted inside an anechoic chamber, approximately 8 m^3 in internal size, lined with acoustic wedges (Sonex) with an absorption coefficient higher than 0.99 for frequencies above 400 Hz. The microphone was mounted on an arm that pivoted around an axis passing through the center of the jet exit. This arrangement enabled sound measurement at a variety of radial r and polar ψ positions. The setup is shown in Fig. 2. For each measurement, the power spectrum was computed according to

$$S(f) = S_{\text{raw}}(f) + \Delta S_{\text{fr}}(f) + \Delta S_{\text{ff}}(f, \phi) \tag{1}$$

where $S_{\text{raw}}(f)$ is the raw spectrum of p'/p_{ref} ($p_{\text{ref}} = 20\ \mu$Pa), $\Delta S_{\text{fr}}(f)$ is the frequency-response correction, $\Delta S_{\text{ff}}(f, \phi)$ is the free-field correction, and ϕ is the angle between the sound propagation vector and the microphone axis that for the present experiments was 0 deg. The sound pressure level (SPL) spectrum is given by

$$\text{SPL}(f) = 10 \log_{10} S(f) \tag{2}$$

and the overall sound pressure level (OASPL), which describes the contribution of all measured frequencies, is computed from the integral

$$\text{OASPL} = 10 \log_{10} \int_0^\infty S(f)\, \mathrm{d}f \tag{3}$$

III. Experimental Results

The coaxial jet flow operating conditions for which calculations were conducted and experimental data were collected are shown in Table 1. The first three cases (CM1, CM2, and CM3) were chosen such that they all have the same mass flow, thrust, and exit area. These types of conditions were recommended by Tanna[11] for comparing noise results of different coaxial jets. For supersonic coaxial jets with a higher-speed primary stream surrounded by a lower-speed secondary stream, the condition of perfect expansion set the primary stream Mach number to the design Mach number of the nozzle. The remaining operating conditions for these cases, referred to as the constant flow condition cases, were found by iteration, subject to an additional criterion of holding the static temperature ratio constant between the two jet streams, until all cases had the same mass flow and thrust for the given coaxial nozzle exit area. The static temperature ratio was determined to be $T_2/T_1 = 0.62$. Hence, the primary variable parameter for the constant flow condition cases is the velocity ratio between the streams. The last three cases (CT1, CT2, and CT3) were chosen to vary only the outer jet stream velocity while holding constant the other fundamental jet flow operating conditions. For these cases, $T_2/T_1 = 0.83$.

Table 2 Averaged gas properties and convective Mach numbers for supersonic coaxial jet calculations

Case	$\bar{\gamma}$	$\bar{R}$, m^2/s^2/K	$\bar{T}_1/T_\infty$	$\bar{T}_2/T_\infty$	M_{c2-1}	M_{c2-2}
CM1	1.56	285.3	3.04	1.89	0.46	1.08
CM2	1.54	292.9	2.65	1.65	0.97	0.76
CM3	1.48	304.3	1.81	1.23	1.54	0.29
CT1	1.62	273.9	3.31	2.77	1.40	0.37
CT2	1.63	275.1	3.29	2.79	1.09	0.80
CT3	1.63	275.3	3.28	2.80	0.93	1.02

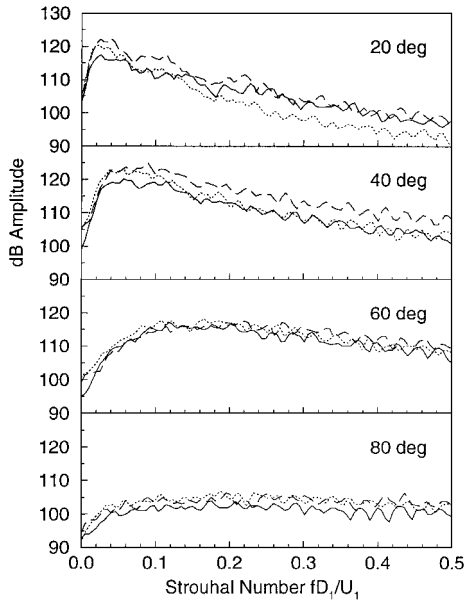

Fig. 3 SPL spectra measured at $r/D_1 = 80$ and at four angles from the downstream jet axis; three constant flow cases: ——, CM1; · · ·, CM2; and – – –, CM3.

In performing the stability and noise calculations, the mean flow for the coaxial jet was provided by the method of Dahl and Morris.[8] The experiments used a mixture of gases to simulate the effects of temperature by changing the gas mixture density. Each stream then had its own gas constant and ratio of specific heats. The mean flow code, however, was designed for a single type of gas with varying temperature. Thus, to complete the mean flow calculations, both an average gas constant and an average specific heat ratio were used with the result that temperature ratios were slightly different from those used in the experiments as indicated in Table 2.

Spectra and Levels

Spectra measured at $r/D_1 = 80$ are shown in Fig. 3 for the three constant flow condition cases at four angles from the exit axis, ψ, in Fig. 2. (Note that, in the context of large distances from the jet, the spherical radius shown in Fig. 2 is used. Otherwise, the radius r is the cylindrical coordinate measured from the jet exit axis.) The data are plotted in terms of a Strouhal number $Sr = fD_1/U_1$ over the range 0–0.5. The spectra have similar shapes for all three conditions. At low angles, there is a well-defined peak at lower Strouhal numbers. The 20-deg spectra peak at about $Sr = 0.04$, and the 40-deg spectra peak at about $Sr = 0.06$. As the angle increases, the peak becomes broader and moves to higher Strouhal number so that at 60 deg, the peak is at about $Sr = 0.14$. Finally, at 80 deg, the spectra have broadened out until there is no clear peak shown for the data when plotted on this scale.

The OASPL for each of the six coaxial jet cases are shown in Table 3 as a function of the measurement angle to the jet axis. The trend of the constant flow cases is a decrease in OASPL as the velocity ratio increases. If we extrapolate to a velocity ratio of 1.0, or the equivalent single jet with the same mass flow, thrust, and exit area, then these normal velocity profile jets are noisier than the equivalent single jet. These results agree with the conclusions given by Tanna.[11]

Table 3 OASPL[a] at four directivity angles

Case	20 deg	40 deg	60 deg	80 deg
CM1	129.5	133.7	133.3	123.5
CM2	130.9	136.3	134.9	125.9
CM3	133.3	138.2	134.8	125.8
CT1	132.8	138.8	137.8	129.1
CT2	133.6	139.0	138.1	130.8
CT3	133.7	137.8	138.7	130.2

[a]In decibel at $80D_1$, referred to 20 μPa.

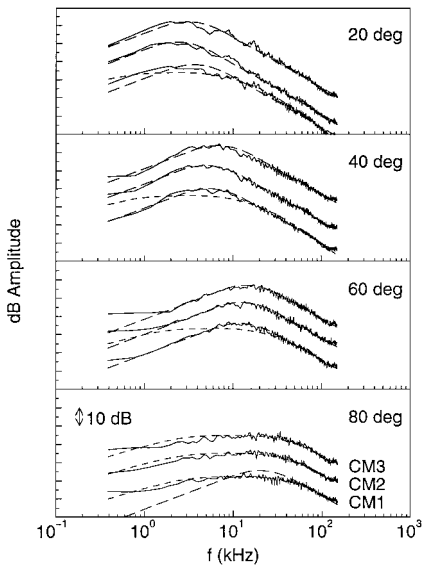

Fig. 4 SPL spectra measured at $r/D_1 = 80$ for the constant flow cases compared to jet noise similarity spectra given in Ref. 16: ——, measured data; – – –, large-scale turbulent structure noise similarity spectrum; and - - - -, fine-scale turbulence noise similarity spectrum.

Spectral Behavior

The spectral behavior, shown in Fig. 3, was previously found in data taken on subsonic coaxial jets[12] and on supersonic coaxial jets that contained shocks.[13] Single, $M = 2$, perfectly expanded supersonic jets also showed this behavior.[14] Stone et al.[15] developed an empirical model for coaxial jet noise prediction using the experimental observation that spectra have a similar shape between single and coaxial jets with a normal velocity profile. The peaks of the coaxial jet spectra were shifted in frequency and direction due to the velocity and temperature ratio changes between the two streams. Recently, Tam et al.[16] correlated the spectral measurements from a large number of single-stream jets to derive a pair of similarity spectra that characterized the two types of turbulent mixing noise. One spectrum had a broad peak and characterized the noise from fine-scale mixing. The other spectrum had a narrower, well-defined peak. It characterized the noise from large-scale mixing. Based on compressibility arguments, they stated that both noise generating mechanisms could exist to some degree in both subsonic and supersonic jets. Their spectra, either singularly or in combination, agreed well with data from axisymmetric, rectangular, and elliptic single-stream jets (see also Refs. 17 and 18). If we consider the spectral similarity observations used by Stone et al.[15] for both single and coaxial jets and consider the similarity of the measured spectral data shown in Fig. 3, there is no reason why Tam's[16] spectra should not apply as well to coaxial jets.

A comparison between the jet noise similarity spectra and the measured spectra is shown in Fig. 4 for the three constant flow cases and in Fig. 5 for the three constant temperature cases. Figures 4 and 5 each show comparisons at four directivity angles. The shapes of the similarity spectra are predefined. The unknown values are the peak frequency and the peak amplitude. These values were determined by a least-squares fitting of the similarity spectra to the measured data. At 20, 40, and 60 deg, the measured spectra are shown to compare well with the large-scale turbulent mixing noise similarity spectrum. In contrast, an example comparison is shown at these

Table 4 Large-scale similarity spectrum peak frequency at three directivity angles derived from a least-square fit to the measured spectrum

	f_p, kHz		
Case	20 deg	40 deg	60 deg
CM1	3.600 ± 0.333	5.277 ± 0.304	11.793 ± 0.458
CM2	2.339 ± 0.192	4.901 ± 0.314	12.428 ± 0.552
CM3	3.085 ± 0.262	6.743 ± 0.446	14.124 ± 0.582
CT1	2.845 ± 0.232	5.670 ± 0.431	11.244 ± 0.585
CT2	2.847 ± 0.248	5.457 ± 0.459	10.774 ± 0.612
CT3	2.842 ± 0.243	4.981 ± 0.407	9.837 ± 0.543

Table 5 Large-scale similarity spectrum peak amplitude at three directivity angles derived from a least-square fit to the measured spectrum

	A[a]		
Case	20 deg	40 deg	60 deg
CM1	118.3 ± 1.3	120.0 ± 0.7	116.1 ± 0.5
CM2	120.7 ± 1.1	122.8 ± 0.8	117.7 ± 0.5
CM3	122.0 ± 1.1	123.8 ± 0.8	117.0 ± 0.5
CT1	122.7 ± 1.1	125.5 ± 1.0	121.1 ± 0.6
CT2	123.7 ± 1.2	126.0 ± 1.1	121.8 ± 0.7
CT3	123.8 ± 1.2	125.3 ± 1.1	122.5 ± 0.7

[a]In decibel at $80D_1$, referred to 20 μPa.

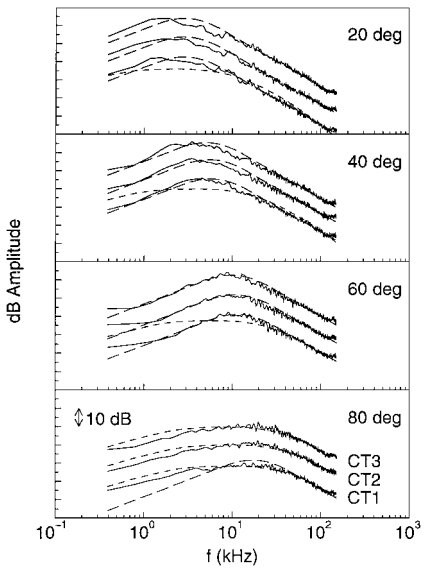

Fig. 5 SPL spectra measured at $r/D_1 = 80$ for the constant temperature cases compared to jet noise similarity spectra given in Ref. 16: ——, measured data; – – –, large-scale turbulent structure noise similarity spectrum; and - - - -, fine-scale turbulence noise similarity spectrum.

angles of a fine-scale turbulent mixing noise similarity spectrum fit to the measured spectrum that does not agree with the measured data at the peak and low-frequency regions. These jets have a supersonic primary stream surrounded by a subsonic to sonic secondary stream, and these results indicate that, in the downstream direction from the jet, noise due to large structures dominates. The results for the least-squares fitting of the peak frequency and peak amplitude are shown in Tables 4 and 5, respectively, for the large-scale similarity spectrum at the lower angles where this spectrum is clearly the dominant shape of the measured data.

At 80 deg, the measured spectra for the constant flow cases, shown in Fig. 4, are no longer characterized by the large-scale similarity spectrum, but are better characterized by the fine-scale similarity spectrum. This result near normal to the jet axis agrees with spectral data comparisons for single stream supersonic jets. However, between directivity angles where the spectral shape is dominated by noise radiated from large-scale turbulent structures and directivity angles where the spectral shape is dominated by noise radiated

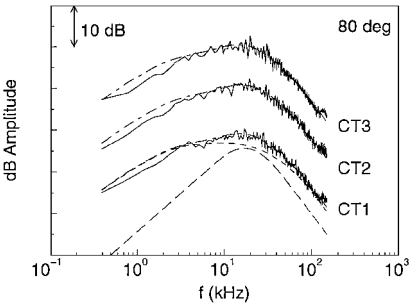

Fig. 6 SPL spectra measured at $r/D_1 = 80$ for the constant temperature cases compared to a combined jet noise similarity spectra based on Ref. 16: ——, measured data; – – –, large-scale turbulent structure noise similarity spectrum; - - - -, fine-scale turbulence noise similarity spectrum; and – – –, combined similarity spectrum.

from fine-scale turbulent mixing are directivities where the spectral shapes are derived from a combination of both large- and fine-scale turbulence-generated noise spectra. The 80-deg angle in Fig. 5 is such a condition for the constant temperature coaxial jet cases. As shown in Fig. 6, the addition of some large-scale structure noise to the fine-scale noise results in a similarity spectrum that better correlates with the measured data, especially in the peak noise region near 20 kHz. Thus, out to an angle of at least 60 deg from the downstream jet axis, the radiated noise is dominated by large-scale structure mixing noise. It is this noise that is modeled using the instability wave noise generation theory. Next, after a brief review of the theory, we will identify the source region for the large-scale structure dominated noise region.

IV. Numerical Calculations

The calculation of the noise radiated from a supersonic jet is based on the linear, inviscid, instability wave theory. A thin free shear layer containing an inflection point in the mean velocity profile is inherently unstable. Initially, an instability wave in the shear layer grows rapidly. This wave growth rate decreases as the shear layer widens until, eventually, the shear layer is too thick to support unstable waves and the wave amplitude decreases until it disappears. The growth and decay of the instability wave produces a range of wave number components. Those components that have a phase velocity that is supersonic relative to the ambient conditions will radiate noise to the far field.

The shear layer of a supersonic jet grows slowly in the axial direction. This slow change in the axial direction compared to more rapid changes in the radial direction allows a locally parallel flow approximation to be used in solving for the disturbance quantities.[4] The governing equations of motion are linearized for small fluctuating disturbances about the mean flow by replacing the instantaneous variables by a sum of a steady mean component and a small fluctuating component, for example, $u = \bar{u} + u'$ for the instantaneous axial velocity, where $\bar{u}$ is the steady mean axial velocity and u' is the small fluctuating quantity. All of the fluctuating disturbance quantities are then represented as waves traveling through a nonuniform medium. For example, the pressure disturbances are given by

$$p'(r, \theta, x, t) = p(r, x) \exp\left\{ i \left[\int_0^x \alpha(\chi)\, \mathrm{d}\chi + n\theta - \omega t \right] \right\} \quad (4)$$

where $p(r, x)$ is the radial r distribution of the pressure disturbance at each axial x location, $\alpha(x)$ is the local complex wave number ($\alpha = \alpha_r + i\alpha_i$ and $-\alpha_i$ is the local growth rate), θ is the azimuthal angle, n is the mode number, and $\exp(-i\omega t)$ is the harmonic time dependence. The linearized equations governing the disturbances can be combined to obtain a single equation,

$$\frac{\partial^2 p}{\partial r^2} + \left(\frac{1}{r} + \frac{2\alpha}{\omega - \alpha\bar{u}} \frac{\partial \bar{u}}{\partial r} - \frac{1}{\bar{\rho}} \frac{\partial \bar{\rho}}{\partial r} \right) \frac{\partial p}{\partial r} + \left(\bar{\rho} M_1^2 (\omega - \alpha\bar{u})^2 - \frac{n^2}{r^2} - \alpha^2 \right) p = 0 \quad (5)$$

This equation has been nondimensionalized by the exit conditions of the primary jet: spatial coordinates by R_1, velocity by U_1, and density by ρ_1. The time and radial frequency are made dimensionless by U_1/R_1 and the pressure by $\rho_1 U_1^2$. To solve Eq. (5) at each axial location, the radial and axial variation of the mean flow velocity $\bar{u}$ and density $\bar{\rho}$ must be known quantities. As stated earlier, these quantities were obtained numerically.[8]

The general solution to Eq. (5) can be written as the sum of two general linearly independent solutions that are functions of the radial and axial coordinates. Outside the jet, the mean flow becomes uniform, and Eq. (5) takes the form of Bessel's equation. This equation is used to enforce the boundary condition that the disturbances generated in the shear layer must decay away from the shear layer, that is,

$$p \sim H_n^{(1)}[i\lambda(\alpha)r] \tag{6}$$

where

$$\lambda(\alpha) = \left[\alpha^2 - \bar{\rho}_\infty M_1^2(\omega - \alpha\bar{u}_\infty)^2\right]^{\frac{1}{2}} \tag{7}$$

and $H_n^{(1)}$ is the nth-order Hankel function of the first kind. At the jet axis, $\partial p/\partial r$ is set to zero for $n = 0$, and $p = 0$ for $n > 0$.

Outside the jet, the governing equations control acoustic disturbances with the same length scales in all directions. The solution to these outer equations is found by Fourier transforming the disturbance variables from the physical axial coordinate x to the wave number coordinate η. The matched asymptotic expansion technique is applied to construct a formula for the pressure disturbances outside the jet generated by the instability wave in the shear layer:

$$p(r, \theta, x, t) = \int_{-\infty}^{\infty} g(\eta) H_n^{(1)}(i\lambda(\eta)r)\, e^{i\eta x}\, e^{in\theta}\, e^{-i\omega t}\, \mathrm{d}\eta \tag{8}$$

where

$$g(\eta) = \frac{1}{2\pi}\int_{-\infty}^{\infty} A_0 \exp\left[i\int_0^x \alpha(\chi)\,\mathrm{d}\chi\right] e^{-i\eta x}\,\mathrm{d}x \tag{9}$$

Equation (9) describes the Fourier transform into wave number space of the axial evolution of the nth mode spatial instability wave at a fixed real frequency ω with unknown initial amplitude A_0. This equation describes the source in a noise radiation problem. Then, Eq. (8) multiplies this source term, $g(\eta)$, by a Hankel function to propagate the generated wave outside the jet and inverts the Fourier transform back to physical space.

Equation (5) and its boundary conditions create an eigenvalue problem for α that is solved using a finite difference approximation. The local eigenvalue is found from the resulting diagonal matrix using a Newton–Raphson iteration technique for refinement yielding the local growth rate $-\alpha_i$ and phase velocity $c_{\mathrm{ph}} = \omega/\alpha_r$. Once α is determined at each axial location, the wave number spectrum is calculated by Eq. (9) followed by the acoustic pressure from Eq. (8). The details for applying this theory to coaxial jets are given in Ref. 1.

V. Numerical Results

Stability Analysis

The results from the stability calculations for the coaxial jet case CM1 are shown in Fig. 7 for the outer shear layer and in Fig. 8 for the inner shear layer. Figures 7 and 8 each show the mean velocity field by outlining the edges of the two potential cores and identify the region over which the two shear layers merge into a single shear layer. The remaining parts of Figs. 7 and 8 show the local phase velocity c_{ph}, the local growth rate $-\alpha_i$, and the instability wave amplitude calculated from the magnitude of the integrand in Eq. (9) when the initial amplitude is set to one. The results shown are for the $n = 1$ mode because this mode typically had the largest wave amplitude.

For the outer shear layer, Fig. 7 shows that the instability wave grows and decays slowly at low Strouhal numbers. The outer shear layer has a larger velocity difference than the inner shear layer and sustains the growth of these longer wavelength instability waves farther downstream to where the shear layers have merged. At higher

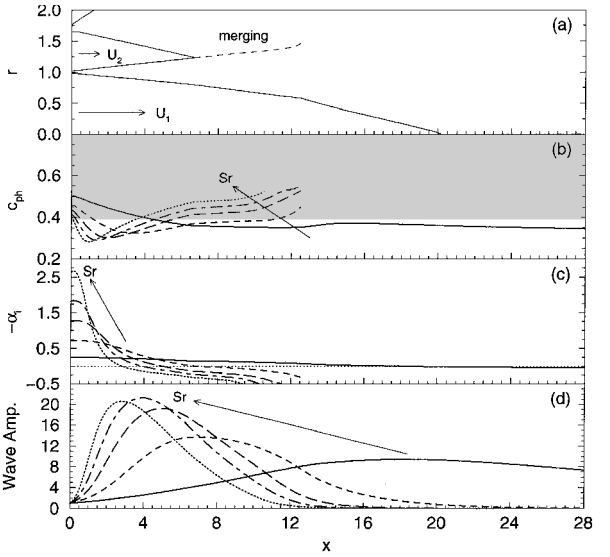

Fig. 7 Stability characteristics for the $n = 1$ mode in the outer shear layer, case CM1. Shaded region indicates phase velocity is supersonic relative to ambient conditions; calculated results for five Strouhal numbers: ——, 0.04; - - - -, 0.12; – – –, 0.20; – - –, 0.28; and · · · ·, 0.40. a) Edges of the shear layers in the velocity field, b) phase velocity relative to U_1 c) growth rate, and d) instability wave amplitude.

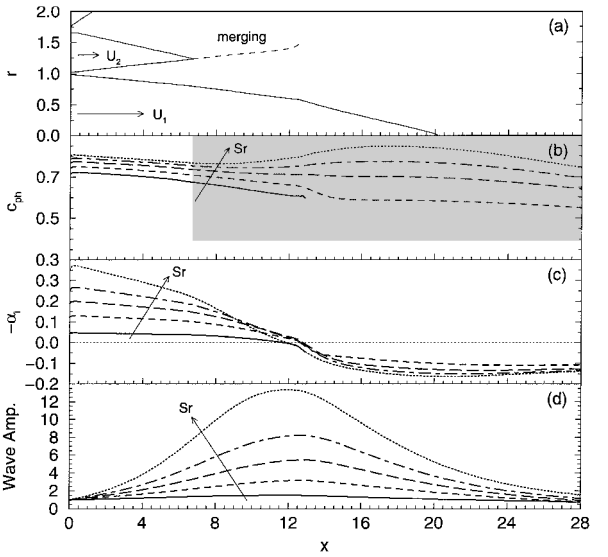

Fig. 8 Stability characteristics for the $n = 1$ mode in the inner shear layer, case CM1. Shaded region indicates phase velocity is supersonic relative to ambient conditions; calculated results for five Strouhal numbers: ——, 0.04; - - - -, 0.12; – – –, 0.20; – - –, 0.28; and · · · ·, 0.40. a) Edges of the shear layers in the velocity field, b) phase velocity relative to U_1 c) growth rate, and d) instability wave amplitude.

Strouhal numbers, the instability wave grows more rapidly and decays more significantly before the outer potential core ends.

The phase velocity varies with the axial distance, first decreasing and then increasing in velocity. According to theory, when the instability wave has a phase velocity that is supersonic relative to the ambient flow, then the wave radiates noise. This criterion is expressed by the general equation

$$|\bar{u}_m - c_{\mathrm{ph}}| > \bar{u}_m/M_m \tag{10}$$

where $m = \infty$ are the ambient flow conditions. Using the flow conditions for the outer shear layer of case CM1 in Eq. (10), we find that when $c_{\mathrm{ph}} > 0.393$, as indicated by the shaded region in Fig. 7b, the phase velocity is supersonic relative to ambient conditions. The outer shear layer instability waves have a short distance during their initial growth, where their phase velocity is supersonic relative to

ambient. However, before they reach peak amplitude, the phase velocity goes subsonic. As the higher-Strouhal-number waves decay, the phase velocity returns to supersonic conditions.

The stability characteristics for the inner shear layer, shown in Fig. 8, are quite different than the outer shear layer stability characteristics. For this case, all of the different Strouhal number modes calculated continue to grow past the end of the outer potential core and do not begin to decay until the inner and the outer shear layers are almost fully merged together. Near the nozzle where the outer potential core still exists, $c_{\text{ph}} > 1.102$ is required for the inner shear layer instability wave phase velocity to be supersonic relative to the secondary flow. [Use $m = 2$ in Eq. (10) to represent the secondary flow conditions.] All of the phase velocities shown in Fig. 8b are subsonic using this criterion. Downstream of the outer potential core, the waves are attaining their maximum amplitude where the shear layers are becoming fully merged. There is only one shear layer in this region, and the phase velocities of the instability waves are now considered relative to ambient conditions. As indicated by the shaded region, we see that the phase velocities are well above 0.393, the condition for supersonic phase velocity relative to ambient and the creation of waves that radiate noise.

From Figs. 7 and 8, we see that an instability wave, growing and decaying in the axial direction, travels through regions with subsonic and supersonic relative phase velocities. This process generates wave number components that may or may not radiate noise to the far field of the jet. To show which components of the instability waves radiate as noise, the wave number spectra calculated by Eq. (9) are shown in Fig. 9a for both the inner and outer shear layer instability waves. As the Strouhal number increases, we see that the wave contains higher wave number content. The condition for far-field noise radiation can be written in terms of the wave number coordinate η, defined in the Fourier transform of the instability wave in Eq. (9), as[1]

$$\eta \leq \frac{\omega}{\bar{u}_\infty + c_\infty / U_1} \tag{11}$$

where c_∞ (meter per second) is the ambient speed of sound. In Fig. 9, the location of the upper limit of Eq. (11) is shown labeled with the Strouhal number. At lower wave numbers (to the left of the indicator), the wave number components radiate noise and at higher wave numbers (to the right of the indicator), the wave number components do not radiate noise. We find that significant portions of the wave number components of the outer shear layer instability

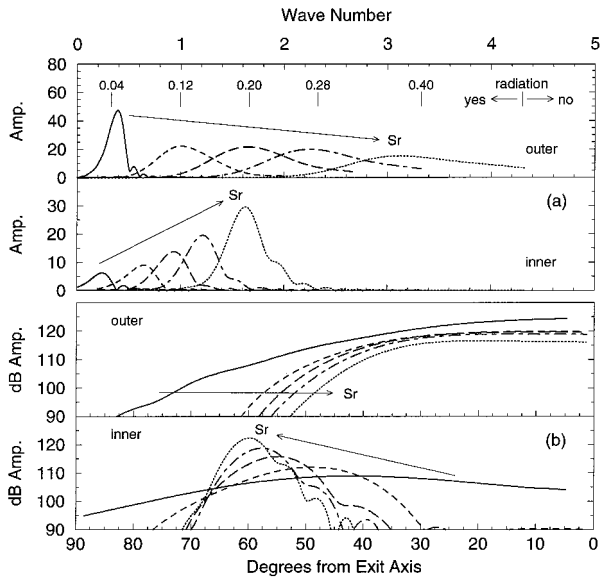

Fig. 9 Case CM1 calculated results for five Strouhal numbers: ——, 0.04; - - - -, 0.12; – – –, 0.20; – – –, 0.28; and · · · ·, 0.40. a) Wave number spectra and upper bound on noise radiation for the wave number components [Eq. (11)] for each Strouhal number and b) radiated noise directivity patterns for the $n = 1$ mode instability waves in the inner and outer shear layers.

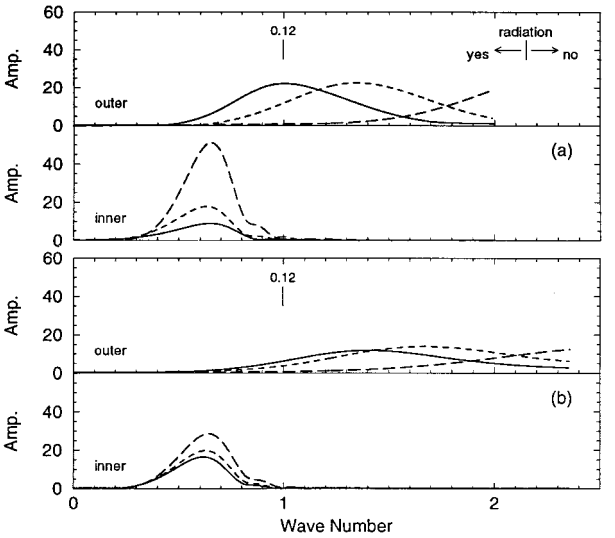

Fig. 10 Wave number spectra for the $n = 1$ mode instability waves, $Sr = 0.12$, inner and outer shear layers and upper bound on noise radiation for the wave number components [Eq. (11)]: a) constant flow conditions ——, $U_2/U_1 = 0.58$; - - - -, $U_2/U_1 = 0.40$; and – – –, $U_2/U_1 = 0.22$; and b) constant temperature conditions ——, $U_2/U_1 = 0.44$; - - - -, $U_2/U_1 = 0.37$; and – – –, $U_2/U_1 = 0.23$.

wave do not radiate noise to the far field. For the inner shear layer, the higher the Strouhal number is, the more the wave number spectrum lies in the region where noise radiation can occur.

Figure 9a represents the wave number spectrum of the noise source. Through the use of Eq. (8), the source is propagated to the far field. Each wave number component defined within the bounds set by Eq. (11) radiates noise to a particular direction in the far field. The wave number component at the upper limit radiates at 0 deg or along the exit axis of the jet. Decreasingly lower wave number components then radiate to increasingly larger directivity angles until at $\eta = 0$, the directivity angle is 90 deg. The resulting directivity patterns are shown in Fig. 9b. Therefore, because the peaks of the noise source spectra of the outer shear layer instability waves lie near the upper limit, that noise is directed downstream of the jet near the axis. In contrast, the inner shear layer has noise sources that radiate at larger angles to the jet exit axis.

The effect of changing the velocity ratio at constant mass flow, thrust, and exit area on the stability characteristics is shown in Fig. 10a. In this example, the wave number spectra at $Sr = 0.12$ are shown for both the inner and the outer shear layer instability waves. As the velocity ratio decreases, the instability wave in the outer shear layer grows and decays more rapidly at a constant Strouhal number, and with lower mean velocities in this shear layer, the phase velocity also decreases resulting in higher wave number components that do not radiate noise to the far field. In contrast, the inner shear layer gets larger, and the wave number components of the instability wave that radiate noise grow larger in amplitude. A similar process is followed by the constant temperature cases shown in Fig. 10b. To varying degrees, the dominance of the inner shear layer instability waves in radiating noise to the far field occurs for all of the Strouhal numbers used in the stability calculations.

Radiated Noise

We now consider the noise radiation characteristics of the instability waves in the coaxial jet compared to measured data. Because the initial amplitude of an instability wave at each frequency and mode is unknown, the comparisons between the measured and the calculated directivities were made by matching the peak amplitude of the calculated directivity to the peak amplitude of the measured directivity obtained from a cubic spline interpolation of the measured data. Hence, the comparisons shown here are qualitative and based on directivity characteristics.

The measured spectral data at seven directivity angles are replotted as a function of the directivity angle at a fixed Strouhal number. The results are shown in Fig. 11 for the three constant flow

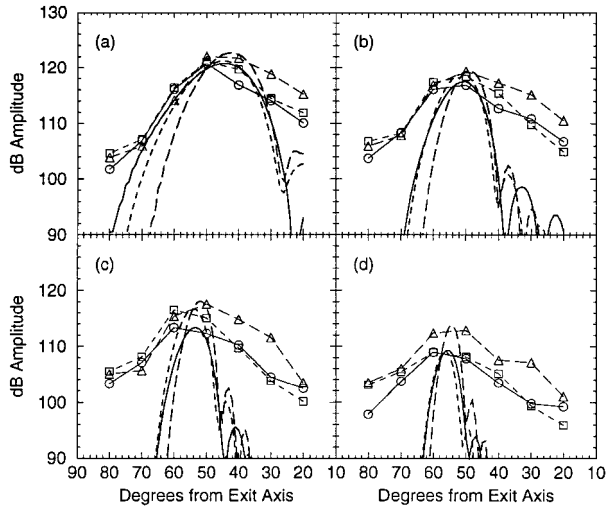

Fig. 11 Comparison of measured directivities (symbols) at $r/D_1 = 80$ to calculated directivities for $n = 1$ mode instability waves in the inner shear layer; constant flow conditions ○ (——), $U_2/U_1 = 0.58$; □ (- - - -), $U_2/U_1 = 0.40$; and △ (– – –), $U_2/U_1 = 0.22$. a) $Sr = 0.12$, b) $Sr = 0.20$; c) $Sr = 0.28$, and d) $Sr = 0.40$.

conditions at four different Strouhal numbers. Clearly, the noise at these Strouhal numbers has a peak directivity in the range from 40 to 60 deg from the jet exit axis. From the spectral comparisons in Fig. 4, the large-scale structures were inferred to be the dominant noise sources radiating to at least a 60-deg angle from the jet exit axis. Furthermore, we showed in Fig. 9 that only the inner shear layer instability waves that continued to grow to their peak amplitude downstream of the outer potential core before decaying radiated noise to large angles away from the jet exit axis. The computed directivities for the four higher-Strouhal-number instability waves originating in the inner shear layer are shown in Fig. 9b to have their peak noise radiated between 40 and 60 deg. This is in contrast to the many instability waves from both the inner and outer shear layers that radiate noise at angles closer to the jet axis. Thus, based on this instability wave analysis, the only large-scale structure or instability wave generated noise that can radiate to the peak directions shown in Fig. 11 for the measured data originate in the inner shear layer. To illustrate this analysis, in Fig. 11 we show the calculated directivity results, from using Eq. (8), for the $n = 1$ mode inner shear layer instability waves that radiate at large angles to the jet axis, for the constant flow cases. The predicted peak directivities are shown to correspond to the measured peak noise region, especially at higher Strouhal numbers. The subtle shifts in directivity that are predicted with increased Strouhal number are also followed by the measured data. As the Strouhal number increases, the peak directivity shifts to higher angles away from the axis.

Figure 11 also shows that the calculated directivities for the $n = 1$ mode correspond with the measured directivities when the velocity ratio U_2/U_1 decreases from 0.58 to 0.22. Dahl and Morris[1] predicted, for a different set of operating conditions, that the effect of decreasing the velocity ratio on inner shear layer instability wave noise radiation is to shift the peak of this noise radiation to lower angles at a given Strouhal number. The measured data for the three constant flow conditions shown in Fig. 11 follow this trend. Dahl and Morris also predicted that the radiated noise levels from the coaxial jets relative to that of the equivalent single jet increase with decreasing velocity ratio. This trend is also followed by the measured data.

The predicted directivity patterns shown in Fig. 11 are much narrower than the measured directivity pattern at the higher Strouhal number. Tam and Chen[7] have shown calculated results for a Mach 2 single jet at a Strouhal number of 0.4, where there are significant contributions to the radiated noise from higher mode number instability waves, thus, broadening the peak. Figure 12 shows an example where the presence of multiple modes may have this effect. Here, the $n = 0$, 1, and 2 modes have been placed on Fig. 12, without regard to their relative level, to show the possibility of broadening the predicted peak directivity pattern. There are other noise sources that

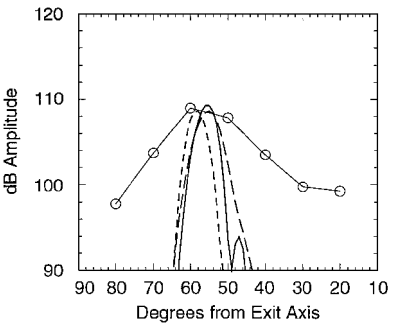

Fig. 12 Comparison of measured directivity (○) at $r/D_1 = 80$ to calculated directivities for three instability wave modes in the inner shear layer of case CM1 at $Sr = 0.40$. Modes: - - - -, $n = 0$; ——, $n = 1$; and – – –, $n = 2$.

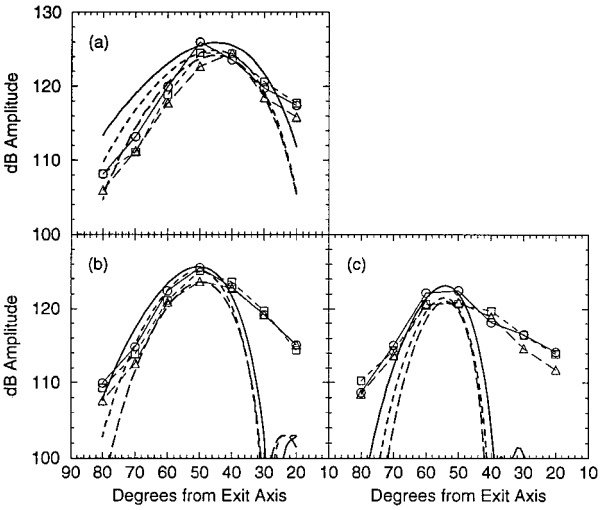

Fig. 13 Comparison of measured directivities (symbols) at $r/D_1 = 80$ to calculated directivities for $n = 1$ mode instability waves in the inner shear layer; constant temperature conditions: ○ (——), $U_2/U_1 = 0.44$; □ (- - - -), $U_2/U_1 = 0.37$; and △ (– – –), $U_2/U_1 = 0.23$. Strouhal number at peak spectral frequency. a) 40 deg, $Sr \approx 0.05$, b) 50 deg, $Sr \approx 0.07$, and c) 60 deg, $Sr \approx 0.10$.

also contribute to the broadening of the directivity pattern including the instability wave generated noise from the outer shear layer that radiates to angles near the axis and the fine-scale mixing noise that is dominant closer to 90 deg from the axis. Research is continuing on the prediction of the relative contributions of these noise sources.

A final set of directivity comparisons are shown in Fig. 13 for the constant temperature cases. The calculations were performed using the Strouhal numbers that correspond to the peak frequencies for the spectra shown in Fig. 5 at 40 and 60 deg and at 50 deg. The measured data show that the peak spectral level in a particular direction does not necessarily correspond to the peak level in the directivity pattern. In Fig. 5, the peak level at 60 deg occurs at $Sr \approx 0.1$. Figure 13c shows that the peak in directivity most likely occurs between 50 and 60 deg, which corresponds well with the predicted directivity. In contrast at 50 deg, the peak spectral level corresponds with the peak in the directivity pattern. Finally, for these constant temperature cases, the direction of the peaks in the directivity patterns change little as the velocity ratio changed in contrast to the shifts that occurred for the constant flow cases; though in the latter cases, the greatest changes in directivity are seen to occur between when $U_2/U_1 = 0.22$ and the two larger-velocity-ratio cases at constant flow conditions, shown in Fig. 11. Nonetheless, for both sets of conditions, the measured directivity at these large angles correspond to the predicted directivities.

VI. Conclusion

The measured noise spectra, generated by the supersonic coaxial jets in this study, can be characterized by the same similarity

spectra that Tam et al.[16] used to characterize single-stream supersonic jets. Even though this characterization is remarkable, we have analyzed just a few of the large possible number of coaxial jet operating conditions and nozzle geometries; thus, it is not possible to generalize that the noise spectra generated by all other coaxial jets can be characterized by these single jet similarity spectra. Nonetheless for the coaxial jet cases presented, where the primary jet stream is supersonic and perfectly expanded and the secondary jet stream is either sonic or subsonic, the agreement of the measured spectra with the large-scale turbulent structure similarity spectrum showed that large-scale structures generated the noise that dominates in the downstream direction. The numerical calculations that followed after these spectral comparisons were used to identify the source region for the noise from the large-scale structures that generated these identifiable spectra.

Using instability waves to model the large-scale structures, we computed the stability characteristics for both the inner and the outer shear layers that were used to determine the axially growing and decaying behavior of the instability waves. These waves represented a noise source that was used to compute the directivity of the sound radiated by each wave toward the ambient region outside of the jet. The noise from the outer shear layer instability waves radiated toward the axis of the jet, whereas the noise from the inner shear layer instability waves radiated in directions up to 60 deg from the jet axis. The measured directivities for Strouhal numbers from 0.12 to 0.4 showed peak directivities in the range from 40 to 60 deg from the jet axis. Because the measured spectrum of the noise in these directions was dominated by large-scale structure or instability wave-generated noise, we inferred from the instability wave noise generation analysis that this noise was generated by instability waves originating in the inner shear layer and reaching their maximum amplitude downstream of the outer potential core where the two shear layers merge. When the coaxial jet operating conditions had the same constant total thrust, mass flow, and exit area, the peak noise direction for these instability waves shifted to lower angles to the jet axis as the velocity ratio decreased. The measured noise directivity followed this trend. Thus, the measured data on the peak noise radiation direction and that on the shift of the peak direction with operating condition changes were both consistent with the behavior of the directivity computed for the noise radiated from the inner shear layer instability waves in a supersonic coaxial jet.

References

[1]Dahl, M. D., and Morris, P. J., "Noise from Supersonic Coaxial Jets, Part 2: Normal Velocity Profile," *Journal of Sound and Vibration*, Vol. 200, No. 5, 1997, pp. 665–699.

[2]Papamoschou, D., "Mach Wave Elimination in Supersonic Jets," *AIAA Journal*, Vol. 35, No. 10, 1997, pp. 1604–1611.

[3]Papamoschou, D., and Debiasi, M., "Noise Measurements in Supersonic Jets Treated with the Mach Wave Elimination Method," *AIAA Journal*, Vol. 37, No. 2, 1999, pp. 154–160.

[4]Tam, C. K. W., and Burton, D. E., "Sound Generated by Instability Waves of Supersonic Flows. Part 2. Axisymmetric Jets," *Journal of Fluid Mechanics*, Vol. 138, 1984, pp. 273–295.

[5]Tam, C. K. W., Chen, P., and Seiner, J. M., "Relationship Between Instability Waves and Noise of High-Speed Jets," *AIAA Journal*, Vol. 30, No. 7, 1992, pp. 1747–1752.

[6]Seiner, J. M., Bhat, T. R. S., and Ponton, M. K., "Mach Wave Emission from a High-Temperature Supersonic Jet," AIAA Paper 93-0734, 1993.

[7]Tam, C. K. W., and Chen, P., "Turbulent Mixing Noise from Supersonic Jets," *AIAA Journal*, Vol. 32, No. 9, 1994, pp. 1774–1780.

[8]Dahl, M. D., and Morris, P. J., "Noise from Supersonic Coaxial Jets, Part 1: Mean Flow Predictions," *Journal of Sound and Vibration*, Vol. 200, No. 5, 1997, pp. 643–663.

[9]Tam, C. K. W., and Hu, F. Q., "On the Three Families of Instability Waves of High-Speed Jets," *Journal of Fluid Mechanics*, Vol. 201, 1989, pp. 447–483.

[10]Hixon, R., Shih, S. H., and Mankbadi, R. R., "Effects of Coannular Flow on Linearized Euler Equation Predictions of Jet Noise," AIAA Paper 97-0284, 1997.

[11]Tanna, H. K., "Coannular Jets—Are They Really Quiet and Why?," *Journal of Sound and Vibration*, Vol. 72, No. 1, 1980, pp. 97–118.

[12]Tanna, H. K., and Morris, P. J., "The Noise from Normal-Velocity-Profile Coannular Jets," *Journal of Sound and Vibration*, Vol. 98, No. 2, 1985, pp. 213–234.

[13]Bassiouni, M. R., and Dosanjh, D. S., "Acoustic and Flow Characteristics of Cold High-Speed Coaxial Jets," *AIAA Journal*, Vol. 17, No. 2, 1979, pp. 153–159.

[14]Seiner, J. M., Ponton, M. K., Jansen, B. J., and Lagen, N. T., "The Effects of Temperature on Supersonic Jet Noise Emission," *Proceedings of the DGLR/AIAA 14th Aeroacoustics Conference*, Vol. 1, Deutsche Gesellschaft für Luft- und Raumfarht, Bonn, 1992, pp. 295–307.

[15]Stone, J. R., Groesbeck, D. E., and Zola, C. L., "Conventional Profile Coaxial Jet Noise Prediction," *AIAA Journal*, Vol. 21, No. 3, 1983, pp. 336–342.

[16]Tam, C. K. W., Golebiowski, M., and Seiner, J. M., "On the Two Components of Turbulent Mixing Noise from Supersonic Jets," AIAA Paper 96-1716, 1996.

[17]Tam, C. K. W., "Jet Noise: Since 1952," *Theoretical and Computational Fluid Dynamics*, Vol. 10, 1998, pp. 393–405.

[18]Tam, C. K. W., "Influence of Nozzle Geometry on the Noise of High-Speed Jets," *AIAA Journal*, Vol. 36, No. 8, 1998, pp. 1396–1400.

M. Samimy
Associate Editor